

Phase retrieval by designed Hadamard complementary coded apertures

Bastián Romero^a, Pablo Scherz^b, Nelson Díaz^a, Jorge Tapia^c, Aarón Cofré^b, Eduardo Peters^d, Esteban Vera^a, Darío G. Pérez^{b,*}

^aEscuela de Ingeniería Eléctrica, Pontificia Universidad Católica de Valparaíso, Av. Brasil 2950, 234-0025, Valparaíso, Chile

^b*Instituto de Física, Pontificia Universidad Católica de Valparaíso, Av. Universidad 330, 234-0000, Valparaíso, Chile*

^cDepartamento de Física, Universidad Técnica Santa María, Av. España 1680, Valparaíso, 2390123, Chile

^dUniversidad de los Andes, Monseñor Álvaro del Portillo 12455, 815-0513, Santiago, Chile

Abstract

Phase retrieval is a challenging inverse problem where amplitude and phase are estimated from diffracted intensities, with applications ranging from microscopy to astronomy. Current computational imaging techniques employ random complementary coded apertures to recover complex optical fields, but require at least 20 masks for effective reconstruction, limiting real-time applications. We propose a novel approach using eight binary Hadamard complementary coded apertures designed to minimize the condition number, thereby ensuring a well-conditioned inverse problem. Our method significantly reduces acquisition time while enhancing reconstruction quality. Using the Fresnel propagation regime and the hybrid input-output algorithm, we validate our approach through extensive simulations with 23 Kodak dataset images across various noise levels. Results demonstrate that our Hadamard approach outperforms conventional random coded methods in reducing the required number of masks. Furthermore, experimental results confirm our technique successfully recovers both simple phase objects like lenses and complex arbitrary phases displayed on spatial light modulators, achieving superior visual quality measured by naturalness image quality evaluation metrics compared to conventional patterns.

Keywords: Phase retrieval, coded illumination, complementary

Hadamard-coded aperture, Fienup hybrid input-output (HIO) algorithm, condition number.

• Introduction

The development of *phase retrieval (PR)* began with the classic Gerchberg-Saxton algorithm, proposed in 1972, which established the fundamental relationship between imaging and diffraction planes using Fourier transforms [1]. Fienup [2] advanced this work in 1978 by incorporating an iterative update function and

*Corresponding author

Preprint submitted to Optics & Laser Technology
Email addresses: bastian.romero@pucv.cl (Bastián Romero), june 13, 2025
pablo.scherz.c@mail.pucv.cl (Pablo Scherz), nelson.diaz@pucv.cl (Nelson Díaz),
jorge.tapiaf@usm.cl (Jorge Tapia), aaron.cofre@pucv.cl (Aarón Cofré),
eduardo.peters@mkuandes.cl (Eduardo Peters), esteban.vera@pucv.cl (Esteban Vera),
dario.perez@pucv.cl (Dario G. Pérez)

14 implementing spatial domain constraints, such as non-negativity and support
15 constraints. These constraints effectively restricted the solution space by enforcing
16 physical conditions that the reconstructed object must satisfy, enabling more
17 reliable convergence. Fienup’s approach gained wide adoption, particularly in
18 X-ray crystallography [3–5], where it provided crucial insights into molecular
19 and crystalline structures. Subsequently, these techniques expanded beyond
20 X-ray applications [6] into various laser-based investigations, though predomi-
21 nantly remained constrained to far-field (Fraunhofer) diffraction scenarios [7, 8],
22 limiting their applicability in near-field imaging problems.

23 In 2011, Candès, Strohmer, and Voroninski introduced the *PhaseLift algorithm*,
24 which can resolve phase retrieval problems by leveraging diffraction
25 patterns under both Fresnel and Fraunhofer conditions (near and far fields)
26 through matrix completion [9, 10]. One of the primary strategies for enhancing
27 phase retrieval performance is incorporating support constraints or, as proposed
28 in [11, 12], multiple constraints using a set of random complementary coded
29 apertures (RCCAs). These coded apertures are the most commonly used be-
30 cause they sample the object via a Bernoulli distribution, ensuring that each
31 pixel is sampled at least once when a sufficient number of apertures is em-
32 ployed [11]. A comprehensive mathematical analysis of the advantages of coded
33 apertures (CAs) can be found in [13]. Recently, this technique has been extended
34 in [14, 15] to enhance efficiency and accelerate the recovery of complex fields,
35 where the overlap between the coded apertures is adjusted to values other than
36 50%, yielding better results compared to conventional random complementary
37 conditioning. However, random mask patterns tend to be ill-conditioned, as the
38 generated diffraction patterns often contain redundancies, reducing the avail-
39 ability of new information in iterative reconstructions. This limitation presents
40 a key challenge in phase retrieval: minimizing the number of iterations required
41 for accurate complex wavefront reconstruction, which is crucial for real-time
42 sensing applications.

43 *Coded diffraction illumination* recovers the phase information of an object
44 by analyzing the Fourier transform of a diffraction intensity image, enhancing
45 information content through probe beam size reduction and oversampling of the
46 speckle pattern. This strategically increased data redundancy helps prevent am-
47 biguous or underdetermined reconstructions. Despite its advantages—such as
48 robustness to noise and low-complexity reconstruction algorithms [16–18]—one
49 significant limitation is the inherent restriction in field of view [17]. The tech-
50 nique of *coded illumination* addresses this issue by modulating the incoming field
51 with multiple coded apertures [18], thus overcoming the trade-off between noise
52 robustness and computational complexity. This approach provides particular
53 advantages in techniques such as ptychography [16]. As a practical example,
54 lensless imaging systems utilizing coded illumination have employed three bi-
55 nary intensity masks in the far-field propagation regime [17].

56 Extending coded illumination imaging to the near field presents two key
57 challenges for phase retrieval applications. First, using binary random coded
58 apertures generates significant redundancy, requiring a large number of aper-
59 tures to recover the complex field. While non-binary masks could theoretically

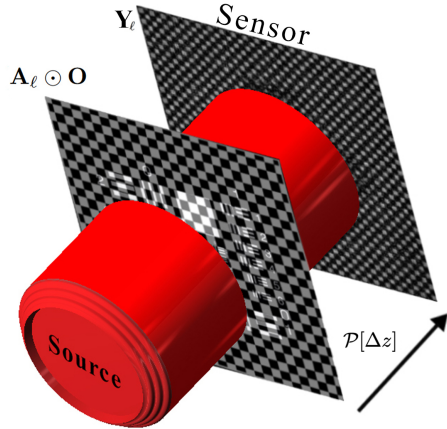


Figure 1: Schematic representation of the coded illumination system for compressive phase retrieval. A coherent wavefront from the complex object \mathbf{O} is modulated by the ℓ^{th} coded aperture \mathbf{A}_ℓ , propagates a distance z in free space, and produces the intensity measurement \mathbf{Y}_ℓ according to Eq. (3). This measurement contains phaseless information that is used in the phase retrieval algorithm.

reduce this redundancy, practical implementation considerations favor binary approaches—digital micromirror devices can achieve switching speeds up to 22 kHz, whereas *liquid crystal on silicon* (LCoS) modulators operate 2-3 orders of magnitude slower. Second, the iterative nature of phase retrieval algorithms imposes time constraints on reconstructions, making it impractical for real-time complex-field wavefront sensing applications. This computational latency renders the technique unsuitable for adaptive optics, where wavefront correction must occur at frequencies on the order of 1 kHz.

In 2008, Hadamard matrices [19] were applied for the first time in the context of compressed sensing for single-pixel imaging [20, 21]. Building on this mathematical foundation, we propose a novel set of coded apertures based on the Hadamard complementary type, which enables faster, more accurate, and reliable reconstructions compared to random complementary coded apertures. Our methodology employs the hybrid input-output algorithm for phase retrieval, combining elements of both Gerchberg-Saxton and Fienup's approaches [2], specifically applied to Fresnel propagators, as detailed in Sec. 2. We demonstrate our approach through both simulations and experiments conducted with real data in Sec. 3. The paper concludes in Sec. 4 with a discussion of the findings and suggestions for future research directions.

2. Coded illumination in the near-field

Figure 1 illustrates the coded illumination process. A collimated coherent beam illuminates an object, producing an unknown complex wavefront \mathbf{O} . This wavefront is encoded by a set of coded apertures, denoted as \mathbf{A}_ℓ , where $\ell =$

83 1, 2, ..., L , representing a total of L measurements. The encoding process is
 84 represented as $\mathbf{A}_\ell \odot \mathbf{O}$, where \odot denotes the Hadamard product. After free-
 85 space propagation over a distance Δz along the z axis, a diffraction pattern \mathbf{I}_ℓ
 86 reaches an image sensor. This can be mathematically expressed as

$$\mathbf{I}_\ell = \mathcal{P}[\Delta z] \{ \mathbf{A}_\ell \odot \mathbf{O} \}, \quad (1)$$

87 where $\mathbf{I}_\ell, \mathbf{O} \in \mathbb{C}^{d \times d}$ and $\mathbf{A}_\ell \in \{0, 1\}^{d \times d}$, with $d \times d$ denoting the number
 88 of pixels in the CA. The operator $\mathcal{P}[\Delta z]$ represents the near-field propagator,
 89 defined [22, 23] by the convolution

$$\mathbf{U}(u, v) = \left[\frac{e^{ik\Delta z}}{i\lambda\Delta z} e^{i\frac{k}{2\Delta z}(u^2 + v^2)} \right] \otimes \mathbf{U}_0, \quad (2)$$

90 where $\mathbf{U}(u, v)$ is the field at the observation plane with coordinates (u, v) , and
 91 \mathbf{U}_0 is the field at the source plane with coordinates (x, y) . Here, λ denotes the
 92 wavelength of the source, and $k = 2\pi/\lambda$ is the wavenumber.

93 Therefore, the ℓ^{th} coded measurement of the diffraction pattern, recorded at
 94 the image sensor, is proportional to the absolute square of the complex wave-
 95 front,

$$\mathbf{Y}_\ell = |\mathbf{I}_\ell|^2 + \boldsymbol{\Omega} \quad (\boldsymbol{\Omega} \in \mathbb{R}^{d \times d}), \quad (3)$$

96 where $|\cdot|$ represents the element-wise modulus operator, and $\boldsymbol{\Omega}$ is an additive
 97 noise term in the real domain $\mathbb{R}^{d \times d}$. Before explaining the nature of the mea-
 98 surement, we can describe the complex object reconstruction as the optimization
 99 problem:

$$f(\mathbf{O}) = \|\mathbf{Y}_\ell - \mathbf{A}_\ell(\mathbf{O}\mathbf{O}^H)\|_2^2, \quad (4)$$

100 where \mathbf{Y}_ℓ is the phaseless data, \mathbf{A}_ℓ is the coded aperture and \mathbf{O} is the complex
 101 signal to be recovered [24]. To obtain a well-conditioned inversion problem, we
 102 need to find a subset L of coded apertures \mathbf{A} that minimizes the correlation
 103 between the measurements \mathbf{Y}_ℓ . Hadamard matrices are well known for gen-
 104 erating maximal sets of pairwise independent random variables with uniform
 105 measure [25]. Each element $(\phi_{ij}) \in \mathbb{R}^{N \times N}$ of a Hadamard matrix takes one of
 106 two values, $\phi_{ij} = 1$ or -1 , and the columns are orthogonal [26]. These proper-
 107 ties are satisfied when $N = 2^M$ for some M . By mapping the entries $\{1, -1\}$ to
 108 $\{1, 0\}$, a non-negative matrix is obtained [27, 28].

109 The proposed coded aperture set is constructed by selecting column vectors,
 110 $\phi_\ell \in \mathbb{R}^{N \times 1}$ with $\ell = 1, \dots, L$, from the Hadamard matrix, optimizing for the
 111 lowest condition number. Given $\Phi_L = [\phi_1 \cdots \phi_L] \in \{0, 1\}^{N \times L}$, we compute the
 112 covariance matrix $\Sigma = \Phi_L^\top \Phi_L$ and minimize its *condition number* (CN), which
 113 is defined as

$$\kappa(\Sigma) = \|\Sigma\| \|\Sigma^{-1}\|,$$

114 where $\|\cdot\|$ represents the l_2 -norm [29, 30]. This minimization criterion provides a
 115 strategy for selecting columns that improve reconstruction quality, independent
 116 of the recovery algorithm used [31].

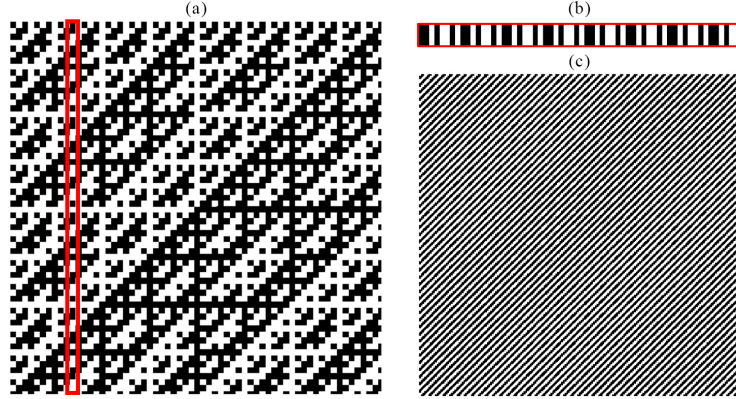


Figure 2: Selection of columns of the Hadamard matrix. (a) Hadamard matrix; (b) chosen column of the Hadamard matrix; (c) resulting Hadamard complementary CA after reshaping the selected column.

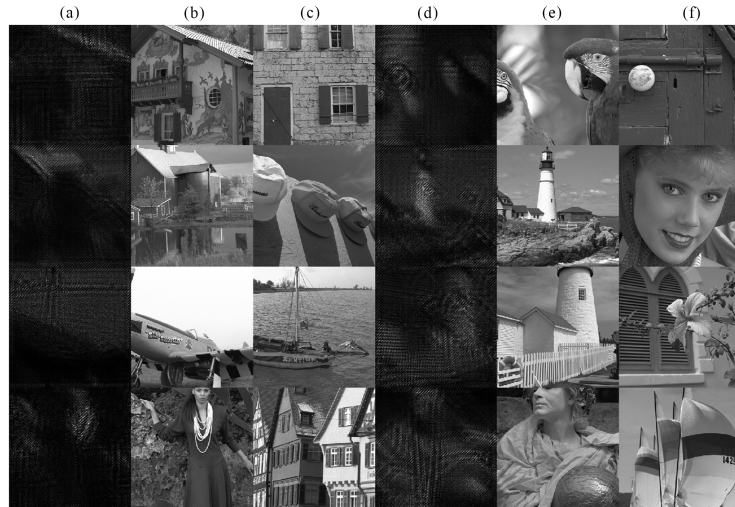


Figure 3: Simulation results using 16 images from the Kodak dataset processed with Hadamard complementary CAs. Each row displays: diffraction patterns from Fresnel propagation in (a) and (d); recovered amplitude of the complex object in (b) and (e); and reconstructed phase of the complex object in (c) and (f).

117 The resulting vectors ϕ_ℓ are reshaped into square binary matrices, $\mathbf{C}_\ell \in$
 118 $\{0, 1\}^{l \times l}$, where $l = \sqrt{N}$. These matrices are then scaled to match the dimen-
 119 sions of the coded apertures, $\mathbf{A}_\ell \in \{0, 1\}^{d \times d}$. Figure 2 illustrates this process,
 120 with the red line indicating the selected column from the Hadamard matrix.

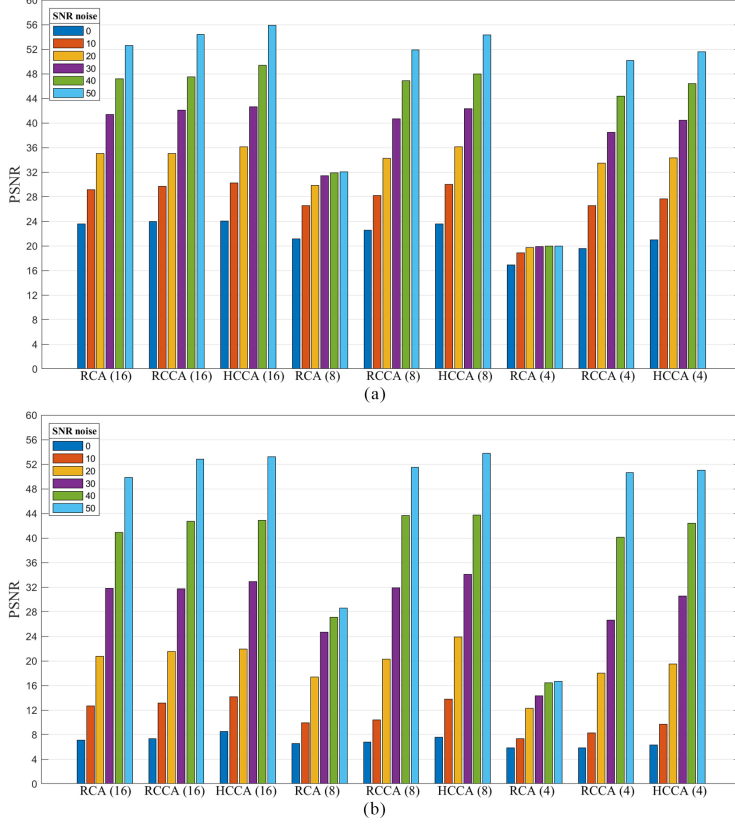


Figure 4: Image quality comparison using peak signal-to-noise ratio (PSNR) across three aperture designs at SNRs ranging from 50 to 0 dB. Results show averaged performance across 23 Kodak dataset images using different aperture quantities: 16 apertures (50 iterations), 8 apertures (150 iterations), and 4 apertures (300 iterations). Subplot (a) displays amplitude PSNR values; subplot (b) shows phase PSNR values.

3. Proof of concept: simulations & experiments

First, to demonstrate how selecting a subset of Hadamard complementary coded apertures that minimizes the condition number increases inference speed and reduces the number of masks required for successful reconstruction, we perform a series of simulations using 23 grayscale images from the Kodak dataset, each with a spatial resolution of $d \times d$ where $d = 384$ [32].

We selected the Hadamard complementary CA set following the procedure outlined in Sec. 2, choosing eight optimal columns from a finite subset of Hadamard matrices. This selection achieved a condition number of 9.053, outperforming the random complementary set which had a CN of 9.096. By including complementary apertures for both sets, we expanded to a total of 16 masks (see Fig. 6, with $N = 2^{15}$ and $d = 384$). Table 1 presents condition number comparisons for different numbers of masks (16 and 8) across three pattern

types: random, random complementary, and Hadamard complementary coded apertures—RCA, RCCA, and HCCA, respectively. The results confirm that our approach consistently achieves lower condition numbers than state-of-the-art methods.

Figure 3 shows simulations where noise is added to the compressive projections, with a signal-to-noise ratio (SNR) of 50 dB. The inputs to the hybrid input-output phase retrieval algorithm are 16 coded measurements, \mathbf{Y}_ℓ , and 16 coded apertures, \mathbf{A}_ℓ , while the outputs of the reconstruction algorithm are the amplitude and phase of the complex object. We simulate the discrete model from Eq.(3) using three aperture types: random with 50% transmittance, random complementary as used in [12], and our proposed Hadamard complementary design. We measure spatial fidelity using peak signal-to-noise ratio.

To simulate more realistic conditions, we add noise to the compressive projections with SN levels of 50, 40, 30, 20, 10, and 0 dB. We compare our approach against both random and random complementary designs with sets of 16, 8, and 4 coded apertures, running 50, 150, and 300 algorithm iterations, respectively. From a theoretical perspective, it has been established [13] that at least two pairs of complementary masks (four masks total) are necessary to guarantee successful phase retrieval in binary coded illumination, making our results with 4 CAs particularly significant. Figure 4 summarizes the results across different mask types and quantities, demonstrating that our approach outperforms the conventional random complementary approach under various noise levels.

To evaluate the performance of our Hadamard complementary CA design under real-world conditions, we implemented an experimental setup for complex-field wavefront sensing, as shown in Fig. 5. This setup employs a pigtailed laser diode ($\lambda = 642$ nm, 20 mW) collimated to produce a 2 cm diameter beam using a lens (L_1 , $f = 500$ mm). A linear polarizer and a half-wave plate between the laser source and collimator adjust the polarization orientation. The collimated beam is sized to match the spatial light modulator (SLM, 1920×1080 px, Jasper Display Corp.) placed behind a beam splitter. Mirror arrangements create a controllable wavefront phase via the SLM. The modulated beam travels through a $4f$ -system to the digital micromirror device (DMD, ViALUX V-7001 VI, 1024×768 resolution, $13.67 \times 13.67 \mu\text{m}^2$ pixel size), which encodes the incoming beam with the predefined coded aperture. After encoding, the beam reflects into an inverted telescope ($M = 1.5$). A field stop between lenses L_4 and L_5 filters out all but the zeroth diffraction order, aligning the pixel sizes of the DMD and the CMOS sensor. Finally, the beam passes through an unknown complex object, propagates freely over a distance of $z = 100$ mm, and reaches the sensor.

Table 1: Comparison of the condition number against the number of coded apertures for the three patterns RCA, RCCA, and HCCA.

Number of Masks	Type of coded aperture		
	RCA	RCCA	HCCA
16	9.1041	9.0965	9.0537
8	5.0229	5.0295	4.9304

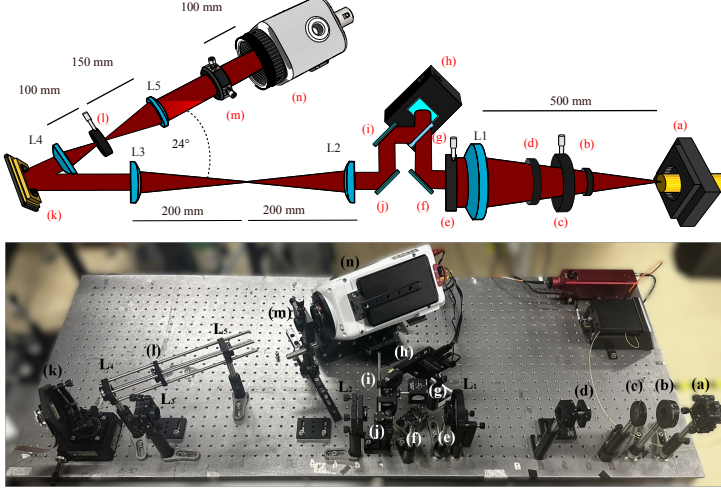


Figure 5: Optical system for phase retrieval using CAs: schematic layout (top) and physical implementation (bottom). It is composed of: a laser light source (a) of $\lambda = 642$ nm propagating through different optical components as a linear polarizer (b); a half-waveplate (d); a collimator lens (L1); field stops (c), (e) and (l); mirrors (f), (i) and (j); a beam splitter (g); an SLM-LCoS (h); a 4f-system composed of lenses (L2) and (L3); an SLM-DMD (k); a $1.5 \times$ telescope system composed of lenses (L4) and (L5); a testing object (m) placed in a plane conjugated with the LCoS and DMD devices; and finally through a CMOS camera (n).

173 We synchronized the high-speed camera (Phantom v611, 12-bit, $20 \mu\text{m}$ pixel
 174 size) with the DMD in a master-slave configuration, selecting a 384×384 pixel
 175 region to match our coded aperture dimensions. These apertures use binary
 176 masks where values of 0 or 1 correspond to micro-mirror tilts of $+12^\circ$ or -12° on
 177 the DMD, with 1s reflecting light and 0s blocking it. Due to the diagonal tilt axis
 178 alignment, we rotated both the DMD and camera 45° around the propagation
 179 axis. Additionally, we tilted the normal axis of the DMD by 24° relative to the
 180 original optical axis to modulate the incoming field into the camera.

181 Based on our simulation results, Fig. 4, we conducted experiments using only
 182 random and Hadamard aperture designs. We loaded each set of L apertures
 183 into the DMD memory and captured corresponding measurements \mathbf{Y}_ℓ for each
 184 aperture pattern \mathbf{A}_ℓ at a rate of 1 kHz. For experimental tests, we employed the
 185 same amplitude masks (Hadamard complementary and random complementary)
 186 used in our simulations, positioning them in the conjugate plane to replicate
 187 realistic imaging conditions.

188 Our reconstructions were performed with both complete aperture sets and
 189 reduced sets of only eight apertures. With complete sets, we conducted 100
 190 iterations to reconstruct the complex objects. The random complementary ap-
 191 proach yielded incomplete amplitude recovery with noticeable darker regions
 192 compared to the Hadamard complementary results. The phase reconstruction
 193 also exhibited significant errors, particularly in central regions that correlated
 194 with amplitude defects, Fig. 7. The Hadamard approach demonstrated faster

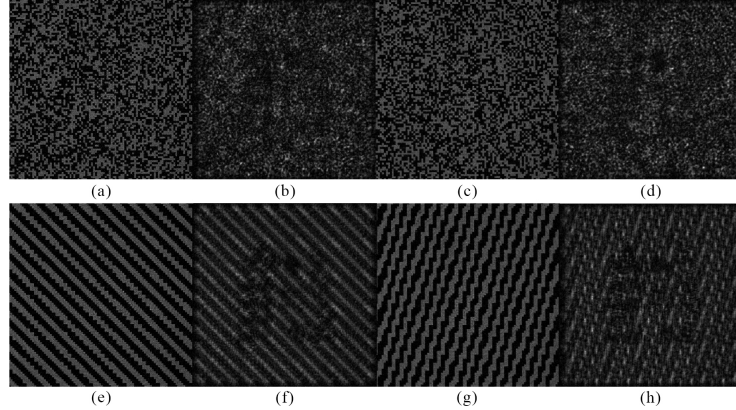


Figure 6: Comparison of aperture patterns in the conjugate plane and their resulting diffraction speckle patterns. Random CA (a,c) and their corresponding diffraction image (b,d); Hadamard CA (e,g) and their corresponding diffraction image (f,h).

195 convergence and greater accuracy, maintaining its superior performance even
196 when we introduced quadratic phase using an $f = 1000$ mm lens.

197 When using the reduced set of eight apertures, Fig. 8, 1500 iterations were

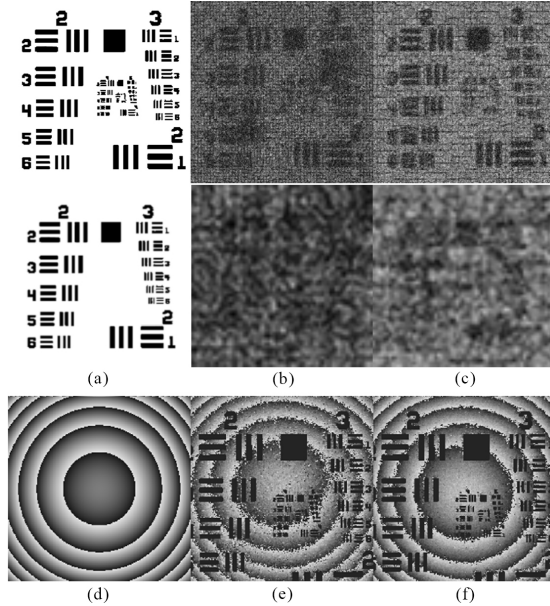


Figure 7: Experimental results using 16 coded apertures and 100 iterations: (a) ground truth amplitude, USAF 1951 mask; (b) reconstruction using RCCA; (c) reconstruction using HCCA; (d) ground truth phase, $f = 1000$ mm lens; (e) phase reconstruction using RCCA; (f) phase reconstruction using HCCA.

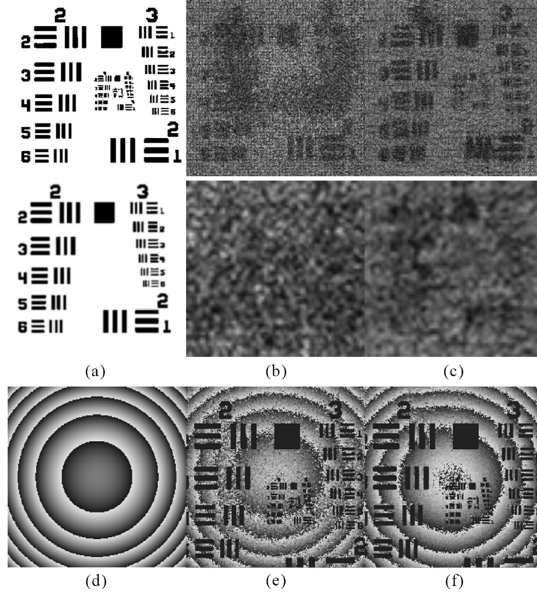


Figure 8: Experimental results using 8 coded apertures and 1500 iterations: (a) ground truth amplitude, USAF 1951 mask; (b) reconstruction using RCCA; (c) reconstruction using HCCA; (d) ground truth phase; (e) phase reconstruction using RCCA; (f) phase reconstruction using HCCA.

necessary for complex object reconstruction. With this reduced set, the random complementary approach produced results lacking detail and exhibiting shape distortion in amplitude recovery. While its phase reconstruction remained similar to that achieved with the full aperture set, accuracy was still inferior. The Hadamard complementary approach consistently outperformed the random approach, delivering more detailed reconstructions of both amplitude and phase components.

To objectively evaluate algorithm convergence under these conditions, we employed the *naturalness image quality evaluator* (NIQE) metric [33], which measures deviations from statistical characteristics found in undistorted natural images. This no-reference metric is particularly suitable for analyzing complex optical fields, with lower scores indicating better quality. Figure 9 shows results from 300 iterations for 16-CA sets and 2500 iterations for 8-CA sets, with the extended iteration count for the latter allowing thorough convergence assessment. These results confirm that the Hadamard complementary approach achieves superior performance by converging in fewer iterations.

Furthermore, we tested the capability of our Hadamard complementary CA approach in reconstructing more complex arbitrary phases and amplitudes. We displayed a portrait of a woman from the Kodak dataset and two Zernike modes (primary spherical aberration and oblique trefoil) on the SLM to introduce varying phase profiles. The USAF 1951 mask served as the amplitude component in

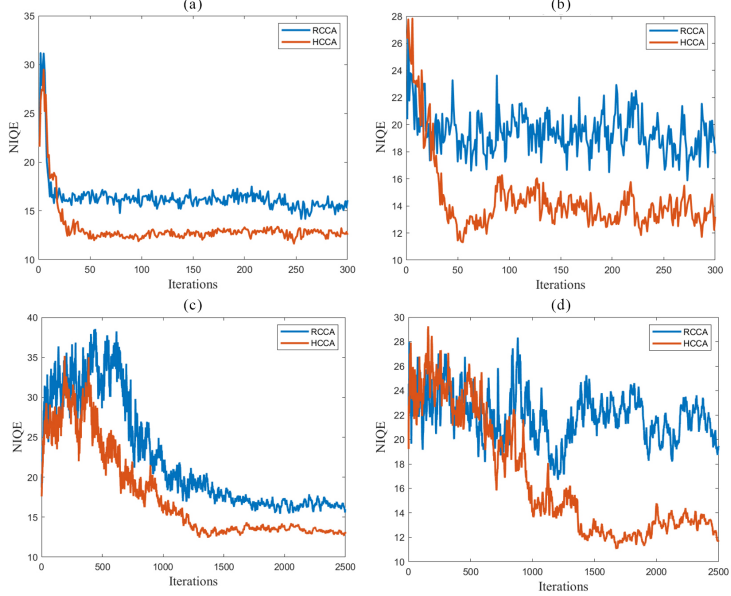


Figure 9: Quality comparison via the NIQE between random and Hadamard complementary CAs for 8 and 16 apertures: (a) amplitude reconstruction with 16 coded apertures; (b) phase reconstruction with 16 coded apertures; (c) amplitude reconstruction with 8 coded apertures; (d) phase reconstruction with 8 coded apertures. Lower NIQE values indicate better image quality

these tests. Figure 10 presents the reconstructed amplitudes and phases for all three test cases. These results demonstrate that our Hadamard complementary approach successfully recovers non-trivial complex objects, suggesting potential applications for inferring phase maps from inputs containing linear combinations of various phase components.

4. Conclusions

We have introduced novel Hadamard complementary coded apertures for recovering the phase and amplitude of an unknown transmission target by encoding coherent light passing through it and measuring the resulting intensity. Our design presents three key advantages: a reduction in the number of coding masks, robustness to noise, and the ability to recover arbitrary phases. Furthermore, although we used the hybrid input-output algorithm for phase reconstruction in our simulations and experimental tests, our coded aperture design is independent of the specific algorithm employed.

We demonstrated that selecting Hadamard columns to minimize the condition number improves the quality of the reconstructed amplitude and phase images. The condition number, which measures the stability and orthogonality of encoding patterns, serves as a key metric in our coded aperture design. In contrast, random complementary CAs exhibit a higher condition number compared

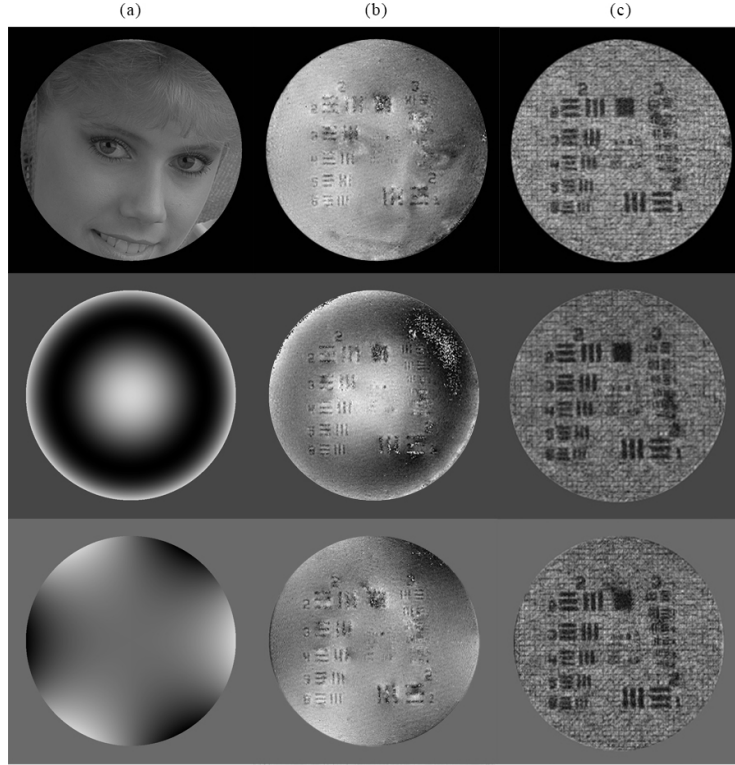


Figure 10: Comparison of reconstruction performance for arbitrary phase profiles with fixed amplitude. The test cases include three different phase distributions: a portrait from the Kodak dataset [32], primary spherical aberration, and oblique trefoil Zernike modes. The amplitude component (USAF 1951 test target) is shown in Fig. 8(a). The figure displays: (a) ground truth phase, (b) reconstructed phase, and (c) recovered amplitude for each test case.

238 to our Hadamard approach. This work shows that the number of measurements
 239 required to recover complex signals is reduced when using carefully designed
 240 patterns.

241 While our validations utilized the hybrid input-output algorithm, the ad-
 242 vantages of our Hadamard complementary approach stem from fundamental
 243 mathematical properties of the measurement operator. This improved condi-
 244 tioning would benefit various phase retrieval methods, including PhaseLift [10],
 245 Wirtinger flow [9], and neural network approaches [24]. This algorithmic versa-
 246 tility makes Hadamard complementary coded apertures valuable across different
 247 computational frameworks and experimental conditions.

248 Our simulations demonstrate that phase and amplitude recovery is possi-
 249 ble with as few as four acquisitions, which aligns with the theoretical min-
 250 imum requirement for binary coded illumination systems [13]. Notably, our
 251 proposed Hadamard complementary design outperforms conventional random
 252 complementary and random CAs at this theoretical minimum. We conducted

extensive simulations across varying noise levels, validated by peak signal-to-noise ratio metrics, to assess the robustness of our design. Real data experiments further confirmed that our Hadamard approach requires only eight coded apertures for phase and amplitude recovery, achieving faster convergence compared to random complementary methods. Notably, the Hadamard approach requires fewer iterations to reach the same visual quality, as evaluated by the naturalness image quality evaluator metric. This improved performance stems directly from the mathematical properties of Hadamard matrices that ensure optimal conditioning of the inverse problem.

Reducing the number of masks used in the reconstruction process, while decreasing acquisition times for real-time implementations, poses a challenging scenario for solving the inverse problem. The binary nature of our approach offers significant advantages in this context, as it enables rapid pattern switching on digital micromirror devices, establishing a foundation for high-speed phase retrieval systems with simplified optical setups. This hardware efficiency must be paired with efforts to minimize the iterations required by the phase retrieval algorithm, primarily through optimization strategies.

One promising direction is the integration of neural network unrolling techniques that exploit initialization to recover the phase using a single mask [34]. Achieving these combined hardware and algorithmic improvements could make this approach faster than other phase retrieval techniques based on coherent light imaging. Such advancements would be particularly valuable in adaptive optics applications requiring wavefront correction, holographic microscopy, and coherent diffraction imaging [35, 36] for studying dynamic biological processes. Additionally, our approach could play a crucial role in optical communication systems [37], where both speed and accuracy in decoding transmitted information are essential.

Acknowledgment

This work was supported in part by Agencia Nacional de Investigación y Desarrollo (ANID), Chile (ANILLO ATE220022; QUIMAL 220006; ALMA 31220004; EXPLORACION 13220234; FONDECYT 1211848; DOCTORADO NACIONAL 2024-21241559; FONDECYT Postdoctorado 3220561); FONDECYT Postdoctorado 3230489.

References

- [1] R. W. Gerchberg and W. O. Saxton, “Practical algorithm for the determination of phase from image and diffraction plane pictures,” *Optik*, vol. 35, no. 2, pp. 237–250, 1972.
- [2] J. R. Fienup, “Reconstruction of an object from the modulus of its Fourier transform,” *Optics letters*, vol. 3, no. 1, pp. 27–29, 1978.
- [3] R. P. Millane, “Phase retrieval in crystallography and optics,” *J. Opt. Soc. Am. A*, vol. 7, pp. 394–411, Mar 1990.

- 294 [4] I. K. Robinson, I. A. Vartanyants, G. J. Williams, M. A. Pfeifer, and J. A.
 295 Pitney, "Reconstruction of the shapes of gold nanocrystals using coherent
 296 X-ray diffraction," *Phys. Rev. Lett.*, vol. 87, p. 195505, Oct 2001.
- 297 [5] B. Abbey, K. A. Nugent, G. J. Williams, J. N. Clark, A. G. Peele, M. A.
 298 Pfeifer, M. De Jonge, and I. McNulty, "Keyhole coherent diffractive imag-
 299 ing," *Nature Physics*, vol. 4, no. 5, pp. 394–398, 2008.
- 300 [6] J. Miao, P. Charalambous, J. Kirz, and D. Sayre, "Extending the method-
 301 ology of X-ray crystallography to allow imaging of micrometre-sized non
 302 crystalline specimens," *Nature*, vol. 400, no. 6742, pp. 342–344, 1999.
- 303 [7] R. A. Gonsalves, "Phase Retrieval And Diversity In Adaptive Optics,"
 304 *Optical Engineering*, vol. 21, no. 5, p. 215829, 1982.
- 305 [8] J. Bertolotti, E. G. Van Putten, C. Blum, A. Lagendijk, W. L. Vos,
 306 and A. P. Mosk, "Noninvasive imaging through opaque scattering layers,"
 307 *Nature*, vol. 491, no. 7423, pp. 232–234, 2012.
- 308 [9] E. J. Candès, Y. C. Eldar, T. Strohmer, and V. Voroninski, "Phase retrieval
 309 via matrix completion," *SIAM Journal on Imaging Sciences*, vol. 6, no. 1,
 310 pp. 199–225, 2013.
- 311 [10] E. J. Candès, T. Strohmer, and V. Voroninski, "Phaselift: Exact and sta-
 312 ble signal recovery from magnitude measurements via convex progra-
 313 mming," *Communications on Pure and Applied Mathematics*, vol. 66, no. 8,
 314 pp. 1241–1274, 2013.
- 315 [11] Z.-J. Cheng, B.-Y. Wang, Y.-Y. Xie, Y.-J. Lu, Q.-Y. Yue, and C.-S.
 316 Guo, "Phase retrieval and diffractive imaging based on babinet's prin-
 317 ciple and complementary random sampling," *Optics Express*, vol. 23, no. 22,
 318 pp. 28874–28882, 2015.
- 319 [12] E. Peters, P. Clemente, E. Salvador-Balaguer, E. Tajahuerce, P. Andrés,
 320 D. G. Pérez, and J. Lancis, "Real-time acquisition of complex optical fields
 321 by binary amplitude modulation," *Optics letters*, vol. 42, no. 10, pp. 2030–
 322 2033, 2017.
- 323 [13] A. Guerrero, S. Pinilla, and H. Arguello, "Phase recovery guarantees from
 324 designed coded diffraction patterns in optical imaging," *IEEE Transactions
 325 on Image Processing*, vol. 29, pp. 5687–5697, 2020.
- 326 [14] C. Xu, H. Pang, A. Cao, Q. Deng, and H. Yang, "Phase retrieval by random
 327 binary amplitude modulation and ptychography principle," *Optics Express*,
 328 vol. 30, no. 9, pp. 14505–14517, 2022.
- 329 [15] O. Bunk, M. Dierolf, S. Kynde, I. Johnson, O. Marti, and F. Pfeiffer, "In-
 330 fluence of the overlap parameter on the convergence of the ptychographical
 331 iterative engine," *Ultramicroscopy*, vol. 108, no. 5, pp. 481–487, 2008.

- 332 [16] M. Li, L. Bian, X. Cao, and J. Zhang, “Noise-robust coded-illumination
 333 imaging with low computational complexity,” *Optics Express*, vol. 27,
 334 no. 10, p. 14610, 2019.
- 335 [17] M. Li, L. Bian, and J. Zhang, “Coded coherent diffraction imaging with
 336 reduced binary modulations and low-dynamic-range detection,” *Optics*
 337 *Letters*, vol. 45, no. 16, p. 4373, 2020.
- 338 [18] M. Li, T. Qin, Z. Gao, and L. Bian, “Illumination schemes for coded co-
 339 herent diffraction imaging: A comprehensive comparison,” *Optics & Laser*
 340 *Technology*, vol. 168, p. 109861, 2024.
- 341 [19] J. Hadamard, “Resolution d’une question relative aux déterminants,” *Bull.*
 342 *des sciences math.*, vol. 2, pp. 240–246, 1893.
- 343 [20] M. F. Duarte, M. A. Davenport, D. Takhar, J. N. Laska, T. Sun, K. F. Kelly,
 344 and R. G. Baraniuk, “Single-pixel imaging via compressive sampling,” *IEEE*
 345 *signal processing magazine*, vol. 25, no. 2, pp. 83–91, 2008.
- 346 [21] G. M. Gibson, S. D. Johnson, and M. J. Padgett, “Single-pixel imaging 12
 347 years on: a review,” *Optics express*, vol. 28, no. 19, pp. 28190–28208, 2020.
- 348 [22] J. W. Goodman, *Introduction to Fourier Optics*. Roberts and Company
 349 Publishers, third ed., 2004. Library.
- 350 [23] J. Schmidt, *Numerical simulation of optical wave propagation: With*
 351 *examples in MATLAB*. SPIE, 01 2010.
- 352 [24] S. Pinilla, K. V. Mishra, I. Shevkunov, M. Soltanalian, V. Katkovnik,
 353 and K. Egiazarian, “Unfolding-aided bootstrapped phase retrieval in op-
 354 tical imaging: Explainable ai reveals new imaging frontiers,” *IEEE Signal*
 355 *Processing Magazine*, vol. 40, no. 2, pp. 46–60, 2023.
- 356 [25] A. Hedayat and W. D. Wallis, “Hadamard matrices and their applications,”
 357 *The annals of statistics*, pp. 1184–1238, 1978.
- 358 [26] J. J. Sylvester, “Lx. thoughts on inverse orthogonal matrices, simultaneous
 359 signsuccesions, and tessellated pavements in two or more colours, with ap-
 360 plications to newton’s rule, ornamental tile-work, and the theory of num-
 361 bers,” *The London, Edinburgh, and Dublin Philosophical Magazine and*
 362 *Journal of Science*, vol. 34, no. 232, pp. 461–475, 1867.
- 363 [27] W. Pratt, *Digital Image Processing*. No. v. 1 in A Wiley-Interscience pub-
 364 lication, Wiley, 1978.
- 365 [28] H. Ryser, *Combinatorial Mathematics*. The Carus Mathematical Mono-
 366 graphs, American Mathematical Society, 1963.
- 367 [29] A. M. Turing, “Rounding-off errors in matrix processes,” *The Quarterly*
 368 *Journal of Mechanics and Applied Mathematics*, vol. 1, pp. 287–308, 01
 369 1948.

- 370 [30] J. R. Rice, “A theory of condition,” *SIAM Journal on Numerical Analysis*,
371 vol. 3, no. 2, pp. 287–310, 1966.
- 372 [31] A. K. Cline, C. B. Moler, G. W. Stewart, and J. H. Wilkinson, “An esti-
373 mate for the condition number of a matrix,” *SIAM Journal on Numerical*
374 *Analysis*, vol. 16, no. 2, pp. 368–375, 1979.
- 375 [32] R. Franzen, “Kodak lossless true color image suite,” source: <http://r0k.us/graphics/kodak>, vol. 4, no. 2, p. 9, 1999.
- 377 [33] A. Mittal, R. Soundararajan, and A. C. Bovik, “Making a “completely
378 blind” image quality analyzer,” *IEEE Signal Processing Letters*, vol. 20,
379 no. 3, pp. 209–212, 2013.
- 380 [34] A. Jerez, J. Estupiñán, J. Bacca, and H. Arguello, “Deep unrolled sin-
381 gle snapshot phase retrieval via non-convex formulation and phase mask
382 design,” *IEEE Journal of Selected Topics in Signal Processing*, pp. 1–10,
383 2024.
- 384 [35] A. E. G. Madsen, M. A. Panah, P. E. Larsen, F. Nielsen, and J. Glückstad,
385 “On-axis digital holographic microscopy: Current trends and algorithms,”
386 *Optics Communications*, vol. 537, p. 129458, 2023.
- 387 [36] S. Marchesini, H. Chapman, S. Hau-Riege, R. London, A. Szoke, H. He,
388 M. Howells, H. Padmore, R. Rosen, J. Spence, et al., “Coherent x-ray
389 diffractive imaging: applications and limitations,” *Optics Express*, vol. 11,
390 no. 19, pp. 2344–2353, 2003.
- 391 [37] M. N’Gom, M.-B. Lien, N. M. Estakhri, T. B. Norris, E. Michielssen, and
392 R. R. Nadakuditi, “Controlling light transmission through highly scattering
393 media using semi-definite programming as a phase retrieval computation
394 method,” *Scientific reports*, vol. 7, no. 1, p. 2518, 2017.